

Article

# The Role of Heterogeneity on Deformation and Flow in Fractured Coal Slopes

Roger Hu <sup>†</sup> and Stuart D. C. Walsh <sup>\*,†</sup>

Civil Engineering, Monash University, Clayton, VIC 3800, Australia

\* Correspondence: stuart.walsh@monash.edu

† These authors contributed equally to this work.

**Abstract:** The fractures in brown coal influence fluid flow and deformation in these materials. These fractures display highly heterogeneous characteristics in the distributions of their apertures, separations and orientations. While discrete fracture models have previously been used to analyse the effects of fractures, such models are not feasible for the scales encountered in many brown-coal mines. Instead, here a continuum permeability model is used to capture the effects of the fracture heterogeneity on fractured coal. This paper presents an analysis of the fracture heterogeneity of brown coal at the AGL Loy Yang coal mine in Latrobe Valley and its influence on the fluid flow, dispersion and rock stability. A stress dependent fracture permeability is considered and captures the effects of heterogeneity in the fracture aperture and orientation. Numerical simulations conducted with multiple plasticity models present different flow paths and potential failure modes depending on the the implemented boundary conditions.

**Keywords:** fractures; hydraulic properties; numerical modelling; fracture strength



check for updates

**Citation:** Hu, R.; Walsh, S.D.C. The Role of Heterogeneity on Deformation and Flow in Fractured Coal Slopes. *Minerals* **2022**, *12*, 1297. <https://doi.org/10.3390/min12101297>

Academic Editor: Stavros Kalaitzidis

Received: 30 August 2022

Accepted: 2 October 2022

Published: 14 October 2022

**Publisher's Note:** MDPI stays neutral with regard to jurisdictional claims in published maps and institutional affiliations.



**Copyright:** © 2022 by the authors. Licensee MDPI, Basel, Switzerland. This article is an open access article distributed under the terms and conditions of the Creative Commons Attribution (CC BY) license (<https://creativecommons.org/licenses/by/4.0/>).

## 1. Introduction

Brown coal slope stability in open-cut mines is greatly influenced by the in situ fracture network and its effect on the flow of fluids within those slopes. The fracture network permits more fluid flow along preferential fracture planes and decreases the overall strength of the material [1]. The fractures also allow for the transmission of fluid contaminants within the slope [2–4]. However, the precise effect of the fracture network on a rock mass may be difficult to characterize due to its heterogeneous nature [5–8].

Several numerical models have been developed to represent the fracture network and simulate its effects on the fluid flow and rock strength. Common approaches include Discrete Fracture Networks and Equivalent Continuum Models. Discrete fracture networks explicitly represent each fracture and their effect on the rock strength and flow properties [9–12]. However, these can be computationally intensive and may require extensive knowledge of the fracture distribution [13].

Instead, modellers often attempt to represent the effects of the fracture network via so-called equivalent or effective continuum models [14,15]. Such models consider the impact of the network on the rock's bulk properties. Nevertheless, in many cases, equivalent-continuum models assume that uniform fracture properties can accurately represent the network's effect on the rock mass [16–18]. Such models often assign a single fracture orientation and strength to simulate the fracture behaviour [19–22]. However, doing so ignores the natural variability of the fracture network.

In this paper, we consider the role that heterogeneity plays in the behaviour of fractured coal slopes. We introduce an effective continuum fracture model that captures the coupling between fluid flow and the mechanical deformation. The model accounts for the spatial heterogeneity in the fracture apertures and orientations by applying sampled distribution values onto each mesh element. This also allows the response of the fracture aperture to mechanical deformation and changes in pore pressure to be modelled by coupling it to the effective normal stress. These fractures are treated as a plane of weakness

with a reduced cohesion and allow for further growth as the pore pressure increases. As some fractures expand more than others depending on their orientation and initial aperture, the effects of the heterogeneity on the network permeability and fluid dispersion are also represented. These models are used to illustrate the effects of the heterogeneous fracture network on the deformation, permeability and fluid dispersion in a block of brown coal.

## 2. Methodology

The following sections outline the coupling between the flow of fluid with the fractured media and its mechanical deformation. More specifically, it describes the calculation of the fracture permeability, the effects of stresses acting upon the fracture-network and the fracture distribution at the AGL Loy Yang brown-coal mine.

### 2.1. Fracture Permeability

The effective continuum permeability model assumes that the overall hydraulic conductivity of the slope is determined by the fracture-network [23]. The permeability of each fracture is represented with the parallel plate approximation:

$$\kappa_{frac} = \frac{h^2}{12}, \quad (1)$$

where  $\kappa_{frac}$  is the permeability of the fracture and  $h$  is the hydraulic aperture [24–28]. However, this does not account for the roughness of the fracture and should be taken as the maximum permeability with given aperture. Nevertheless, the mechanical and hydraulic aperture are almost equivalent for fractures with large apertures [29,30].

A spacing  $d$  between fractures is added to account for a fracture set, the three-dimensional permeability becomes:

$$\kappa_{ij}^{joint} = \frac{h^3}{12d} [\delta_{ij} - n_i n_j] \quad (2)$$

where  $\delta_{ij}$  is the Kronecker delta and  $n_i$  is the fracture normal [31,32]. However, the hydraulic aperture,  $h$ , of the fracture is affected by the stress conditions acting on the fracture network. Several models such as Seidle et al. [33], Liu & Rutqvist [34], Chen et al. [35] and Yan et al. [36] represent this relationship using the following equation:

$$h = h_0 \exp(-C_h \sigma_{eff}), \quad (3)$$

where  $C_h$  is the fracture compressibility,  $h_0$  is the initial hydraulic aperture,  $\sigma_{eff}$  is the effective stress. The effective stress is the difference between the stress acting perpendicular to the fracture and the pore pressure. In addition to this, a normal plastic strain component is added to represent permeability hysteresis that can be observed in fractured rock masses [37–39]. The relationship then becomes:

$$h = h_0 \exp(-C_h \sigma_{eff}) + \epsilon_n d, \quad (4)$$

where  $\epsilon_n$  is the normal plastic strain and  $d$  is the fracture spacing as before. The fracture compressibility measures the change in the fracture porosity based on the stress applied:

$$C_h = \frac{-1}{\phi_f} \frac{\partial \phi_f}{\partial \sigma_{eff}}, \quad (5)$$

where  $\phi_f$  is the fracture porosity [35,40,41]. An extensive review by Tan [42] reports a range of coal fracture compressibility values up to  $0.2 \text{ MPa}^{-1}$  for brown coal. A value of  $0.1 \text{ MPa}^{-1}$  is adopted for the compressibility in this paper.

## 2.2. Fracture Distribution

Probability distributions were fitted to fracture data provided by AGL Loy Yang to represent heterogeneity in the coal fractures. More specifically, log-normal and log-beta distributions yielded excellent representations of the fracture apertures. Figure 1a shows that a majority of the fractures are less than 10 mm, however the small number of large apertures greatly increase the average size. Three Gaussian distributions were fitted to the fracture orientations to account for the multiple joint sets present as shown in Figure 1b. A majority of the fractures are vertical, however there are horizontal bedding planes that exist and need to be considered to account for the heterogeneity. These provide a majority of the horizontal permeability as shown with the minor fracture plane in Figure 1c. Figure 1c represents the distribution of permeability compared to the original raw data from AGL Loy Yang. It considers the effects of the aperture and orientation distributions and shows the permeability in each joint set with significantly higher values in the primary vertical orientation compared to the minor horizontal plane.

The fractures used in Sections 3.1 and 3.2 were sampled off these fitted distributions to provide an accurate representation of the AGL Loy Yang brown-coal mine. More details on the fitted fracture distributions can be found in Hu et al. [43] and Hu and Walsh [44].

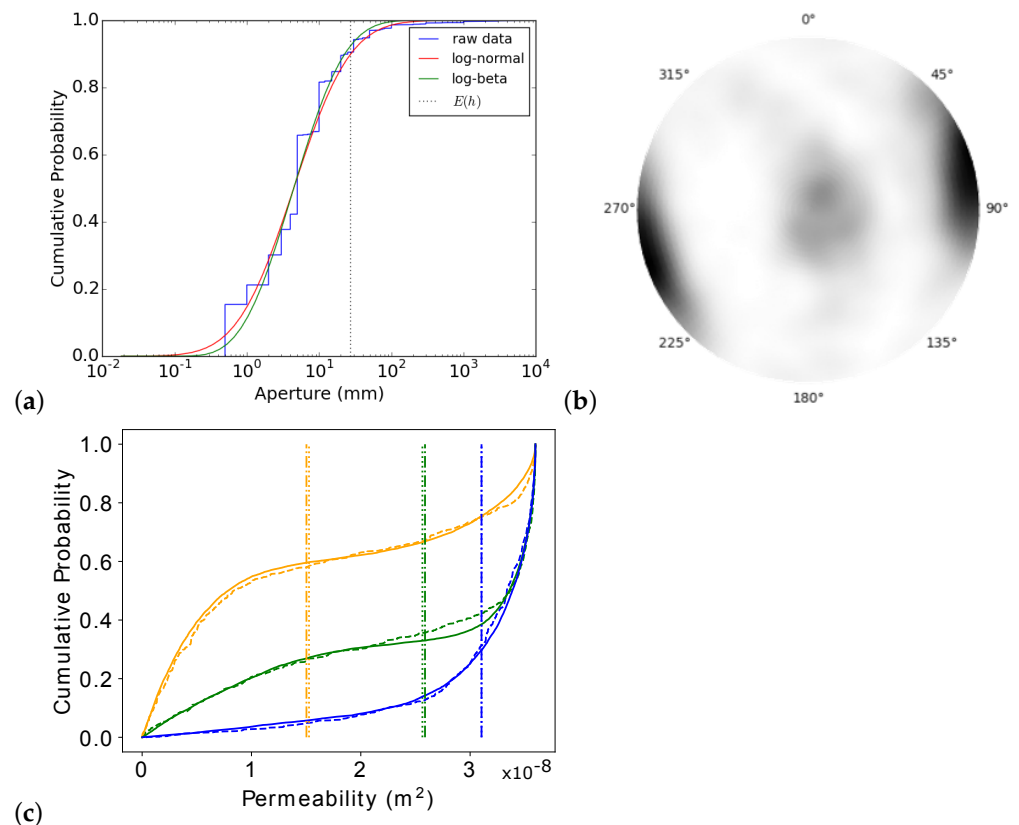


**Figure 1.** The distribution of fracture properties: (a) Log-normal and log-beta distributions fitted to the raw data; (b) a stereonet of the distribution of fracture orientations dominated by vertical fractures; (c) the permeability distribution of each fracture axis accounting for the distribution of apertures and orientations.

## 2.3. Mechanical Properties

In addition to affecting the permeability, the fractures also influence the mechanical strength of the coal [45,46]. We represent this in the model by introducing a weak-plane model that reduces the coal's tensile strength along particular directions. In the model, the planes of weakness are aligned with the same orientations as the local fracture normals that were generated from fitted aperture and spacing probability distributions. The tensile strength of the fractures may be adjusted such that they have zero strength in tension or

such that they are assigned a nominal residual strength. The weak plane failure surface is applied in addition to the regular plastic failure surface for the coal body—allowing the coal to fail along other planes under the appropriate conditions. The Mohr Coulomb plastic failure criterion are applied for the coal body with average brown coal properties. Several studies conducted on the brown coal at Latrobe Valley indicate a cohesion of approximately 0.15 MPa and a friction angle of 30° [47,48]. Nevertheless, these values represent the properties of fractured coal. Instead, to represent the strength of the intact coal as a bulk material, a cohesion of 3 MPa is used based on the range provided by several other studies [46,49,50].

### 3. Results and Discussion

The effects of the fracture distribution were analysed under different confining pressures. Numerical models using the effective continuum model were then simulated to capture the effects of the fracture heterogeneity on fluid flow and plastic strain.

#### 3.1. Confinement Effects on the Permeability

A series of numerical simulations were conducted to understand the effects of the fracture heterogeneity on the system permeability at different confining stresses. The confinement is applied at different depths below surface with an additional in situ stress ratio to represent horizontal confinement. Several studies investigated the horizontal to vertical in situ stress ratio in the Latrobe Valley mines and estimated it to be from 0.4 up to 1 [48,51,52]. A ratio of 0.5 is adopted to represent the AGL Loy Yang brown coal mine. The results of these simulations are then compared with a high in situ stress ratio of 2.0 found in other areas within Australia [53,54]. Depths of 50 m, 100 m, 150 m and 200 m were considered to compare the effects of different confinement under both saturated and unsaturated water conditions.

Numerical simulations were conducted on a block of coal with different applied confining pressures to represent varying depths and in situ stresses. Fluid flow was added to simulate saturated and unsaturated conditions. The average permeability tensor was then extracted from the simulations and plotted as ellipsoids in Figure 2. Figure 2c,d are under saturated conditions. There is minimal change in the orientation and the magnitude of permeability with the increase in depth as the pore pressure caused by the fluid keeps the fractures open. The mean vertical permeability for a 0.5 in situ stress ratio is  $8.3 \times 10^{-6} \text{ m}^2$  at 200 m depth under saturated conditions. This decreases to  $7.6 \times 10^{-6} \text{ m}^2$  under an in situ stress ratio of 2.0. However, this is not the case when the system remains unsaturated. Figure 2a not only shows a decrease in the permeability compared to the saturated conditions but also a change in orientation under 200 m depth. The fracture permeability become more vertical due to a higher vertical pressure closing the horizontal fractures. In contrast, Figure 2b applies greater horizontal stress than the vertical so the orientation does not shift as the fracture network is dominated by vertical fractures. However, there is a larger reduction in the magnitude of permeability due to the higher stresses acting on the vertical fractures. The unsaturated permeability decreases from  $5.5 \times 10^{-6} \text{ m}^2$  to  $4.6 \times 10^{-6} \text{ m}^2$  at 200 m depth with the increase in the in situ stress ratio.

#### 3.2. Numerical Simulations on the Fracture Aperture Heterogeneity

The effects of the fracture network on the dispersion and mechanical deformation of the coal were simulated in the Multiphysics Object-Orientated Simulation Environment (MOOSE) created by Idaho National Laboratory. MOOSE has previously been used to couple numerous physics such as solid mechanics, fluid flow and heat conduction [55–57].

A series of numerical simulations were conducted to capture the effects of the fracture on the dispersion and deformation in coal. Firstly, two simulations were conducted under 200 m confinement with both unsaturated and saturated conditions. Fluid is added in from the left side and allowed to flow out on the right to capture the dispersion caused by the fractures.

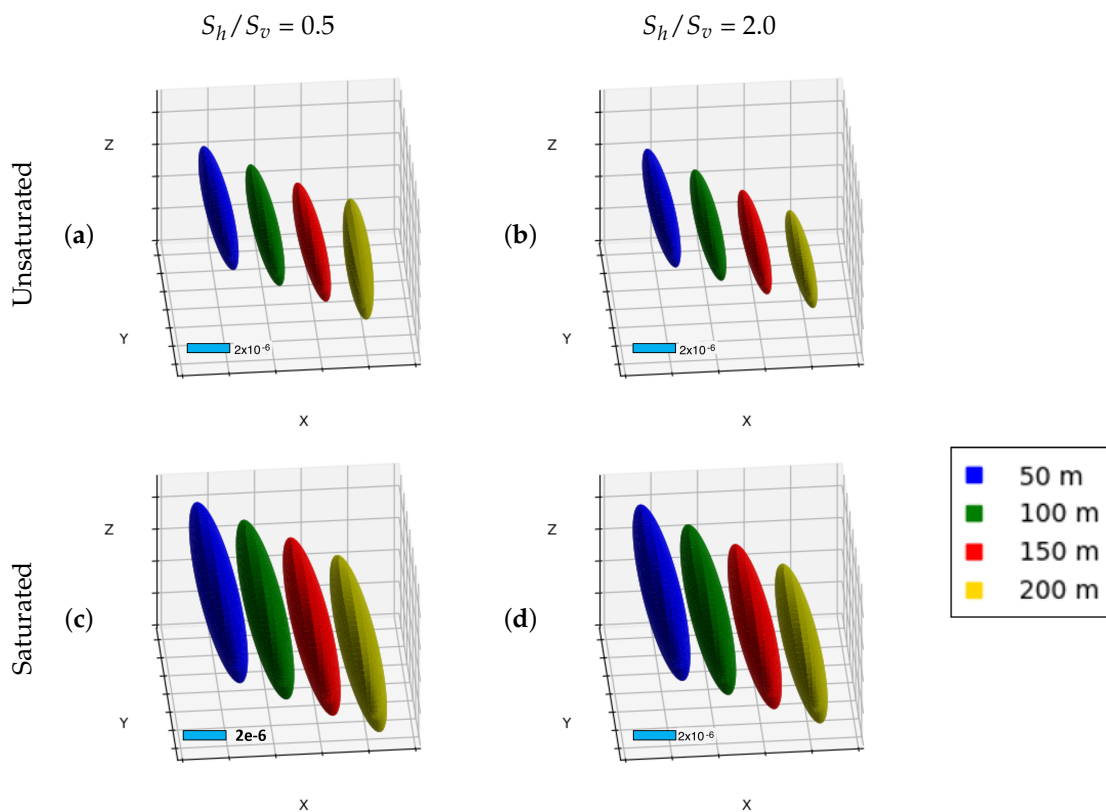


**Figure 2.** The permeability tensors at depths of 50 m, 100 m, 150 m and 200 m plotted as ellipsoids. There is a noticeable change in the permeability magnitude and orientation under unsaturated conditions under different depths as well as between in situ stress ratios of 0.5 (a) and 2.0 (b). There is a small permeability difference under saturated conditions between in situ stress ratios of 0.5 (c) and 2.0 (d). The length of the scale represents a permeability of  $2 \times 10^{-6} \text{ m}^2$ .

In addition to analysing the dispersion, two separate models were used to illustrate the mechanical effects of rainfall in an unsaturated coal block with randomly sampled fracture orientations from the previously fitted distributions in Section 2.2. These models apply a fluid inflow at the surface of the simulation and include a mechanical strength in the fractures and bulk material. The fluid flow is driven by gravity and coupled with the fractures so that the fractures can expand with the decrease in normal stress as shown in Equations (3) and (4). To illustrate the effects the fractures have on the possible failure mechanisms in the model, two scenarios are compared with different degrees of heterogeneous fractures. In the first scenario, the fracture aperture distribution is limited to a range of 20% from the mean aperture size. The second simulation removes this limitation and samples directly from the aperture distribution. A variable flux boundary condition was applied on the surface that permits more fluid flow with larger apertures. The fluid flux gradually increases and will travel towards the ground water table where a constant pore pressure was set at the bottom of the model. The numerical model is fully coupled so the pore pressure will increase as the fluid flows in the block of coal and decrease the effective normal stress acting on the fractures. This allows for the fracture to expand and contract as the simulation progresses.

The resulting streamlines of the random aperture fields under saturated and unsaturated conditions are shown in Figure 3. There is much high retention time of the fluid in the coal under unsaturated conditions. This results in less fluid mobility as shown in Figures 4 and 5. Trend lines with a gradient of 0.5 were fitted to the standard deviations of the log-displacement in Figure 5c,d. The values of the standard deviation is proportional to

the dispersion and can be used to calculate the dispersion in the horizontal and vertical directions by applying the equation:

$$\sigma = \langle \Delta x^2 \rangle^{1/2} = (2Dt)^{1/2} = (2\alpha ut)^{1/2}, \tag{6}$$

where  $\sigma$  is the standard deviation,  $x$  is the displacement,  $D$  is the dispersion,  $t$  is the time,  $\alpha$  is the dispersivity (m) and  $u$  is the average velocity (m/s)

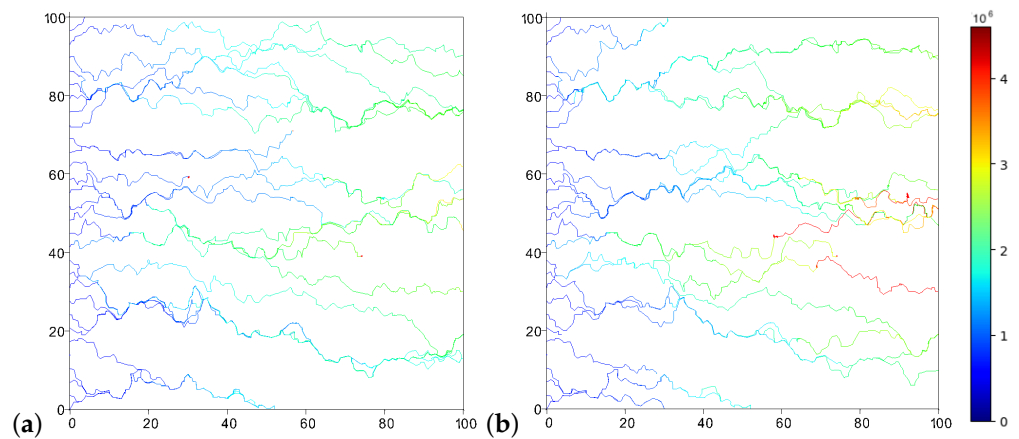


**Figure 3.** Streamlines of the fluid flow under 200 m depth with 0.5 in situ ratios in the 100 m by 100 m block of coal. The fully saturated conditions (a) have a lower retention time (shown in seconds) compared to the unaturated conditions (b).

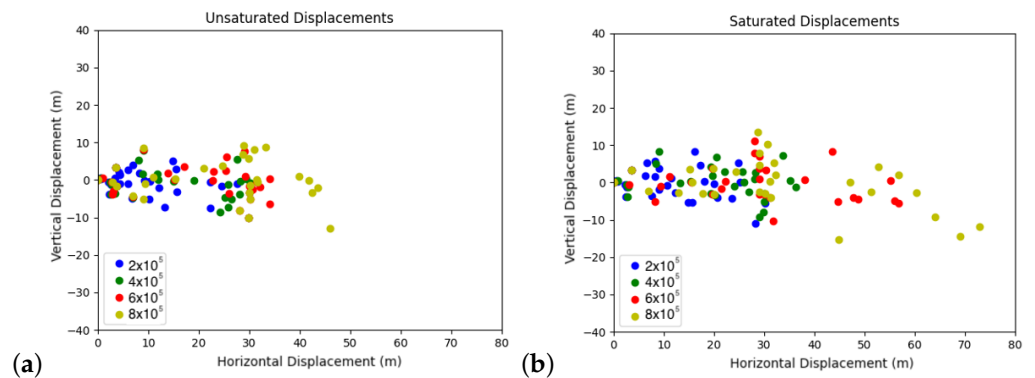


**Figure 4.** Plots of the displacement (shown in meters) of the streamlines sampled at times  $2 \times 10^5$ ,  $4 \times 10^5$ ,  $6 \times 10^5$  and  $8 \times 10^5$  seconds for: (a) Unaturated conditions and (b) Saturated conditions.

There is a higher dispersivity coefficient,  $\alpha$ , in the horizontal ( $x$ ) direction than the vertical as shown by the values calculated in Table 1. This is expected as there is no pressure difference in the vertical axis to force fluid flow, and longitudinal dispersivity is typically greater than transverse dispersivity. However, it should be noted that the vertical dispersivity decreases under saturated conditions, while the horizontal dispersivity tends to increase. This is due to the significantly higher horizontal dispersivity so the horizontal fractures expand more than the vertical. Thus, permitting greater transport in the horizontal direction than the vertical.

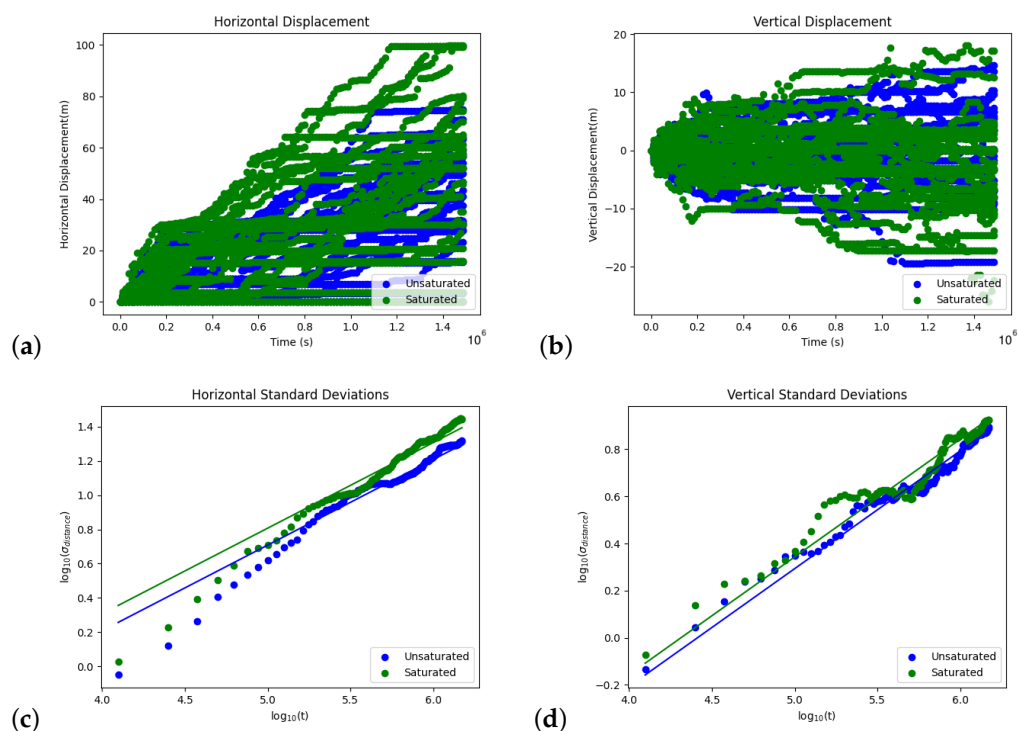


**Figure 5.** Plots showing the: (a) horizontal displacement of the streamlines over time (b) vertical displacement of the streamlines over time; (c) log-standard deviation of the horizontal displacement in the streamlines and (d) log-standard deviation of the vertical displacement in the streamlines.

**Table 1.** The calculated dispersivity in each direction.

	Unsaturated	Saturated
Horizontal Intercept	−1.791	−1.692
Vertical Intercept	−2.206	−2.156
Mean Horizontal Velocity (m/s)	0.000141	0.000216
$\alpha_x$	0.927	0.954
$\alpha_y$	0.137	0.113

The mechanical effects of a random aperture field can be observed in Figure 6. From the beginning of the simulation, the inflow flux is more localised at one location where there is a large aperture. In contrast, the first simulation with a limited aperture distribution presents an even spread of fluid flux and a more uniform spread of pore pressure with lower magnitudes. This inhibits localisation of fluid and build up of pore pressure so the effective compressive normal stresses remain high and no failure occurs. However, when the full extent of the fractures apertures is considered, there is a localisation of fluid flow and deformation matching the predominant fracture orientations at the location of the largest fractures. The concentration of fluid also reduces the effective normal stress in those fractures, allowing them to open up and permit greater amounts of flow. The continuous increase of flow over the course of the simulation in localised regions further reduce the compressive normal stress and permits more fluid flow in these areas. This results in a gradually increasing plastic strain matching the predominant joint orientations in locations of high aperture size. However, the plastic strain and fracture opening is limited to the surface due to increasing compressive forces with depth. There is also a large strength difference between the fractures and the bulk coal material, hence all the plastic strain is attributed to expansion in the fractures.

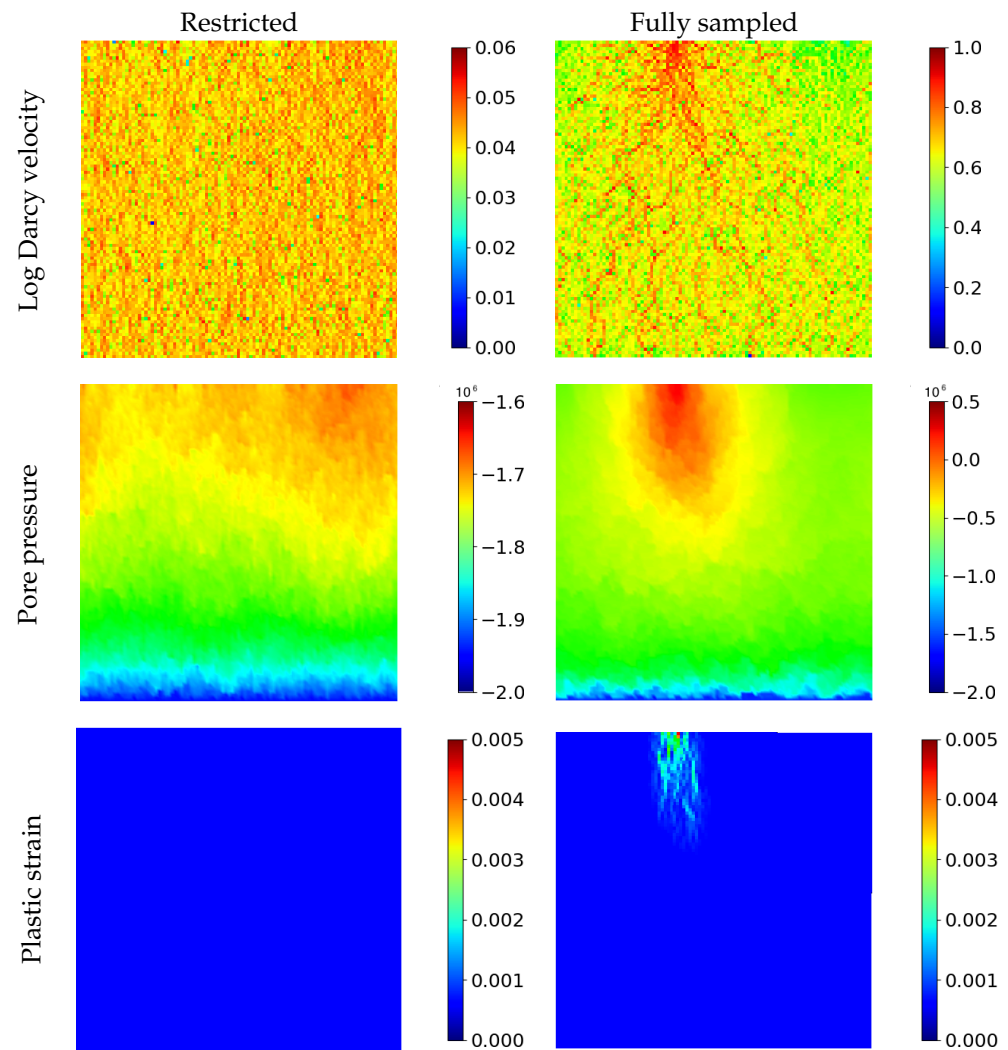


**Figure 6.** Results of the two simulations showing the log-magnitude of Darcy velocity, pore-water pressure and resultant plastic strain with restricted and fully sampled apertures.

#### 4. Conclusions

The ability to capture the effects of heterogeneous fracture networks is important for mining operations that involve highly fractured media, such as brown coal. An effective continuum fracture-network model was presented in this paper that captures the influence of fractures on the mechanical stability and fluid flow in rock formations. The present approach ascribes individual fracture properties to each element, sampled from the underlying probability distributions.

A heterogeneous fracture field with properties based on those observed in a real coal mine was simulated using the model. The results illustrate how different confining pressures affect not only the magnitude of the permeability but also the dominant direction, as some fractures close more than others depending on their orientation. The mechanical behaviour of the heterogeneous fractures was compared with that of a more uniform distribution in response to an applied fluid flux. The heterogeneity presented a case of localised fluid flow reducing the effective stress acting on the fracture and allowing it to expand. This permitted more dispersion in the dominant flow direction as these fractures expanded more. The fluid flow also produced regions of high plastic strain that were not observed in the simulations based on a uniform aperture field. These results indicate that localisation of deformation may not be observed with average properties, instead an accurate distribution of fracture properties must be sampled to observe the effects of heterogeneity to accurately assess the stability of these slopes.

**Author Contributions:** Conceptualization, R.H. and S.D.C.W.; methodology, R.H. and S.D.C.W.; software, R.H.; validation, R.H.; formal analysis, R.H.; investigation, R.H.; resources, S.D.C.W.; data curation, R.H.; writing—original draft preparation, R.H. and S.D.C.W.; writing—review and editing, R.H. and S.D.C.W.; visualization, R.H.; supervision, S.D.C.W.; project administration, S.D.C.W.; funding acquisition, S.D.C.W. All authors have read and agreed to the published version of the manuscript.

**Funding:** Roger Hu was funded by a grant from AGL Loy Yang.

**Data Availability Statement:** The data presented in this study are available on request from the corresponding author. The data are not publicly available due to privacy concerns.

**Acknowledgments:** We gratefully acknowledge the support for this project provided by AGL Loy Yang and the continuing advice and collaboration of Jon Missen and Nicole Anderson.

**Conflicts of Interest:** The authors declare no conflict of interest.

## Abbreviations

The following abbreviations are used in this manuscript:

MOOSE Multiphysics Object-Orientated Simulation Environment

## References

1. Wang, P.; Jiang, L.; Jiang, J.; Zheng, P.; Li, W. Strata behaviors and rock burst-inducing mechanism under the coupling effect of a hard, thick stratum and a normal fault. *Int. J. Geomech.* **2018**, *18*, 04017135. [[CrossRef](#)]
2. Bear, J.; Tsang, C.F.; De Marsily, G. *Flow and Contaminant Transport in Fractured Rock*; Academic Press: Cambridge, MA, USA, 2012.
3. Parker, B.L.; Cherry, J.A.; Chapman, S.W. Discrete fracture network approach for studying contamination in fractured rock. *AQUA Mundi* **2012**, *3*, 101–116.
4. Blessent, D.; Jørgensen, P.R.; Therrien, R. Comparing discrete fracture and continuum models to predict contaminant transport in fractured porous media. *Groundwater* **2014**, *52*, 84–95. [[CrossRef](#)] [[PubMed](#)]
5. Schweiger, H.; Thurner, R.; Pöttler, R. Reliability analysis in geotechnics with deterministic finite elements—Theoretical concepts and practical application. *Int. J. Geomech.* **2001**, *1*, 389–413. [[CrossRef](#)]
6. Hsu, S.C.; Nelson, P.P. Material spatial variability and slope stability for weak rock masses. *J. Geotech. Geoenviron. Eng.* **2006**, *132*, 183–193. [[CrossRef](#)]
7. Song, K.I.; Cho, G.C.; Lee, S.W. Effects of spatially variable weathered rock properties on tunnel behavior. *Probab. Eng. Mech.* **2011**, *26*, 413–426. [[CrossRef](#)]
8. Pandit, B.; Tiwari, G.; Latha, G.M.; Babu, G.S. Stability analysis of a large gold mine open-pit slope using advanced probabilistic method. *Rock Mech. Rock Eng.* **2018**, *51*, 2153–2174. [[CrossRef](#)]
9. Merrien-Soukatchoff, V.; Korini, T.; Thoraval, A. Use of an integrated discrete fracture network code for stochastic stability analyses of fractured rock masses. *Rock Mech. Rock Eng.* **2012**, *45*, 159–181. [[CrossRef](#)]
10. Grenon, M.; Landry, A.; Hadjigeorgiou, J.; Lajoie, P.L. Discrete fracture network based drift stability at the Éléonore mine. *Min. Technol.* **2017**, *126*, 22–33. [[CrossRef](#)]
11. Wang, L.; Chen, W.; Tan, X.; Tan, X.; Yang, J.; Yang, D.; Zhang, X. Numerical investigation on the stability of deforming fractured rocks using discrete fracture networks: A case study of underground excavation. *Bull. Eng. Geol. Environ.* **2020**, *79*, 133–151. [[CrossRef](#)]
12. Zhu, G.; Sousa, R.; He, M.; Zhou, P.; Yang, J. Stability analysis of a non-pillar-mining approach using a combination of discrete fracture network and discrete-element method modeling. *Rock Mech. Rock Eng.* **2020**, *53*, 269–289. [[CrossRef](#)]
13. Yin, T.; Chen, Q. Simulation-based investigation on the accuracy of discrete fracture network (DFN) representation. *Comput. Geotech.* **2020**, *121*, 103487. [[CrossRef](#)]
14. Baek, S.H.; Kim, C.Y.; Kim, K.Y.; Hong, S.W.; Moon, H.K. A numerical study on the effect of heterogeneous/anisotropic nature of rock masses on displacement behavior of tunnel. *Tunn. Undergr. Space Technol.* **2006**, *21*, 391. [[CrossRef](#)]
15. Kong, P.; Jiang, L.; Shu, J.; Sainoki, A.; Wang, Q. Effect of fracture heterogeneity on rock mass stability in a highly heterogeneous underground roadway. *Rock Mech. Rock Eng.* **2019**, *52*, 4547–4564. [[CrossRef](#)]
16. Sitharam, T.; Sridevi, J.; Shimizu, N. Practical equivalent continuum characterization of jointed rock masses. *Int. J. Rock Mech. Min. Sci.* **2001**, *38*, 437–448. [[CrossRef](#)]
17. Gutierrez, M.; Youn, D.J. Effects of fracture distribution and length scale on the equivalent continuum elastic compliance of fractured rock masses. *J. Rock Mech. Geotech. Eng.* **2015**, *7*, 626–637. [[CrossRef](#)]
18. Shin, H.; Santamarina, J.C. An implicit joint-continuum model for the hydro-mechanical analysis of fractured rock masses. *Int. J. Rock Mech. Min. Sci.* **2019**, *119*, 140–148. [[CrossRef](#)]

19. Shojaei, A.; Taleghani, A.D.; Li, G. A continuum damage failure model for hydraulic fracturing of porous rocks. *Int. J. Plast.* **2014**, *59*, 199–212. [[CrossRef](#)]
20. Fernández-Álvarez, J.P.; Álvarez-Álvarez, L.; Díaz-Noriega, R. Groundwater numerical simulation in an open pit mine in a limestone formation using MODFLOW. *Mine Water Environ.* **2016**, *35*, 145–155. [[CrossRef](#)]
21. Gui, Y.L.; Bui, H.H.; Kodikara, J.; Zhang, Q.B.; Zhao, J.; Rabczuk, T. Modelling the dynamic failure of brittle rocks using a hybrid continuum-discrete element method with a mixed-mode cohesive fracture model. *Int. J. Impact Eng.* **2016**, *87*, 146–155. [[CrossRef](#)]
22. Zhang, H.; Huang, Y.; Yang, Z.; Xu, S.; Chen, X. A discrete-continuum coupled finite element modelling approach for fibre reinforced concrete. *Cem. Concr. Res.* **2018**, *106*, 130–143. [[CrossRef](#)]
23. Pruess, K.; Wang, J.; Tsang, Y. On thermohydrologic conditions near high-level nuclear wastes emplaced in partially saturated fractured tuff: 2. Effective continuum approximation. *Water Resour. Res.* **1990**, *26*, 1249–1261.
24. Witherspoon, P.A.; Wang, J.S.; Iwai, K.; Gale, J.E. Validity of cubic law for fluid flow in a deformable rock fracture. *Water Resour. Res.* **1980**, *16*, 1016–1024. [[CrossRef](#)]
25. Zimmerman, R.W.; Bodvarsson, G.S. Hydraulic conductivity of rock fractures. *Transp. Porous Media* **1996**, *23*, 1–30. [[CrossRef](#)]
26. Waite, M.E.; Ge, S.; Spetzler, H.; Bahr, D.B. The effect of surface geometry on fracture permeability: A case study using a sinusoidal fracture. *Geophys. Res. Lett.* **1998**, *25*, 813–816. [[CrossRef](#)]
27. Teng, T.; Gao, F.; Ju, Y.; Xue, Y. How moisture loss affects coal porosity and permeability during gas recovery in wet reservoirs? *Int. J. Min. Sci. Technol.* **2017**, *27*, 899–906. [[CrossRef](#)]
28. Wang, K.; Liu, A.; Zhou, A. Theoretical analysis of influencing factors on resistance in the process of gas migration in coal seams. *Int. J. Min. Sci. Technol.* **2017**, *27*, 315–319. [[CrossRef](#)]
29. Iwai, K. Fundamental studies of fluid flow through a single fracture. Ph.D. Thesis, University of California, Berkeley, CA, USA, 1976.
30. Barton, N.; Bandis, S.; Bakhtar, K. Strength, deformation and conductivity coupling of rock joints. *Int. J. Rock Mech. Min. Sci. Geomech. Abstr.* **1985**, *22*, 121–140
31. Chen, M.; Bai, M.; Roegiers, J.C. Permeability tensors of anisotropic fracture networks. *Math. Geol.* **1999**, *31*, 335–373. [[CrossRef](#)]
32. Snow, D.T. Anisotropic permeability of fractured media. *Water Resour. Res.* **1969**, *5*, 1273–1289. [[CrossRef](#)]
33. Seidle, J.; Jeansonne, M.; Erickson, D. Application of matchstick geometry to stress dependent permeability in coals. In Proceedings of the SPE Rocky Mountain Regional Meeting, Casper, Wyoming, 18–21 May 1992.
34. Liu, H.H.; Rutqvist, J. A new coal-permeability model: Internal swelling stress and fracture–matrix interaction. *Transp. Porous Media* **2010**, *82*, 157–171. [[CrossRef](#)]
35. Chen, D.; Pan, Z.; Ye, Z. Dependence of gas shale fracture permeability on effective stress and reservoir pressure: Model match and insights. *Fuel* **2015**, *139*, 383–392. [[CrossRef](#)]
36. Yan, Z.; Wang, K.; Zang, J.; Wang, C.; Liu, A. Anisotropic coal permeability and its stress sensitivity. *Int. J. Min. Sci. Technol.* **2019**, *29*, 507–511. [[CrossRef](#)]
37. Guvanasen, V.; Chan, T. A three-dimensional numerical model for thermohydrromechanical deformation with hysteresis in a fractured rock mass. *Int. J. Rock Mech. Min. Sci.* **2000**, *37*, 89–106. [[CrossRef](#)]
38. Huo, D.; Benson, S.M. An experimental investigation of stress-dependent permeability and permeability hysteresis behavior in rock fractures. In *Fluid Dynamics in Complex Fractured-Porous Systems*; Wiley: Amsterdam, The Netherlands, 2015; pp. 99–114.
39. Selvadurai, A. Normal stress-induced permeability hysteresis of a fracture in a granite cylinder. *Geofluids* **2015**, *15*, 37–47. [[CrossRef](#)]
40. Zheng, G.; Pan, Z.; Chen, Z.; Tang, S.; Connell, L.D.; Zhang, S.; Wang, B. Laboratory study of gas permeability and cleat compressibility for CBM/ECBM in Chinese coals. *Energy Explor. Exploit.* **2012**, *30*, 451–476. [[CrossRef](#)]
41. Lei, G.; Cao, N.; McPherson, B.J.; Liao, Q.; Chen, W. A novel Analytical Model for pore Volume compressibility of fractal porous Media. *Sci. Rep.* **2019**, *9*, 14472. [[CrossRef](#)]
42. Tan, Y.; Pan, Z.; Feng, X.T.; Zhang, D.; Connell, L.D.; Li, S. Laboratory characterisation of fracture compressibility for coal and shale gas reservoir rocks: A review. *Int. J. Coal Geol.* **2019**, *204*, 1–17. [[CrossRef](#)]
43. Hu, R.; Walsh, S.; Missen, J.; Anderson, N. Simulating fracture network permeability in brown-coal slopes. In Proceedings of the 2020 International Symposium on Slope Stability in Open Pit Mining and Civil Engineering, May 12, 2020; Australian Centre for Geomechanics: Crawley, Australia, 2020; pp. 1281–1290.
44. Hu, R.; Walsh, S.D. Effective Continuum Approximations for Permeability in Brown-Coal and Other Large-Scale Fractured Media. *Geosciences* **2021**, *11*, 511. [[CrossRef](#)]
45. Meng, Z.; Peng, S.; Li, H. Influence of normal faults on the physical and mechanical properties of coal and the distribution of underground pressure. *Mei T'an Hsueh Pao (J. China Coal Soc.)* **2001**, *26*, 561–566.
46. Scholtès, L.; Donzé, F.V.; Khanal, M. Scale effects on strength of geomaterials, case study: Coal. *J. Mech. Phys. Solids* **2011**, *59*, 1131–1146. [[CrossRef](#)]
47. Tolooiyan, A.; Mackay, R.; Xue, J. Measurement of the tensile strength of organic soft rock. *Geotech. Test. J.* **2014**, *37*, 991–1001. [[CrossRef](#)]
48. Narendranathan, S.; Stipceovich, J.; Rastogi, S. A case study: Assessing the impacts of open cut coal mining on the Maryvale Field (Yallourn) Open Cut and Morwell River Diversion through the use of finite element modelling. In Proceedings of the 2020 International Symposium on Slope Stability in Open Pit Mining and Civil Engineering, Crawley, Australia, 12 May 2020; Australian Centre for Geomechanics: Crawley, Australia, 2020; pp. 849–862.

49. Lindsay, P.; Campbell, R.; Fergusson, D.; Gillard, G.; Moore, T. Slope stability probability classification, Waikato coal measures, New Zealand. *Int. J. Coal Geol.* **2001**, *45*, 127–145. [[CrossRef](#)]
50. Zhao, Z.; Wang, W.; Wang, L.; Dai, C. Compression–shear strength criterion of coal–rock combination model considering interface effect. *Tunn. Undergr. Space Technol.* **2015**, *47*, 193–199. [[CrossRef](#)]
51. Barton, C. Regional stress and structure in relation to brown coal open cuts of the Latrobe Valley, Victoria. *J. Geol. Soc. Aust.* **1981**, *28*, 333–339. [[CrossRef](#)]
52. Nag, D. Estimation of in situ stress in the Latrobe Valley Coal mines with special reference to Loy Yang Mine, Australia. In *Computer Applications in the Mineral Industries*; CRC Press: Boca Raton, FL, USA, 2020; pp. 601–606.
53. Mark, C.; Gadde, M. Global trends in coal mine horizontal stress measurements. In Proceedings of the 10th Underground Coal Operators’ Conference, Wollongong, Australia, 11–12 February 2010; University of Wollongong & the Australasian Institute of Mining and Metallurgy: Wollongong, Australia, 2010; pp. 21–39.
54. Karatela, E.; Taheri, A.; Xu, C.; Stevenson, G. Study on effect of in situ stress ratio and discontinuities orientation on borehole stability in heavily fractured rocks using discrete element method. *J. Pet. Sci. Eng.* **2016**, *139*, 94–103. [[CrossRef](#)]
55. Tonks, M.R.; Gaston, D.; Millett, P.C.; Andrs, D.; Talbot, P. An object-oriented finite element framework for multiphysics phase field simulations. *Comput. Mater. Sci.* **2012**, *51*, 20–29. [[CrossRef](#)]
56. Podgorney, R.; Huang, H.; Gaston, D. *Massively Parallel Fully Coupled Implicit Modeling of Coupled Thermal-Hydrological-Mechanical Processes for Enhanced Geothermal System Reservoirs*; Technical Report; Idaho National Laboratory (INL): Idaho Falls, ID, USA, 2010.
57. Wilkins, A.; Green, C.P.; Ennis-King, J. PorousFlow: A multiphysics simulation code for coupled problems in porous media. *J. Open Source Softw.* **2020**, *5*, 2176. [[CrossRef](#)]